Available online at www.sciencedirect.com
SCIENCE DIRECT
Journal of Power Sources 153 (2006) 312–318
JOURNAL OF POWER SOURCES
www.elsevier.com/locate/jpowsour

Thermodynamics and crystal structure anomalies in lithium-intercalated graphite

Rachid Yazami *, Yvan Reynier

CNRS-CALTECH International Associated Laboratory, Materials for Electrochemical Energetics (ME^2), California Institute of Technology, MC 138-78, Pasadena, CA 91125, USA

Available online 8 August 2005

Abstract

We found anomalous behaviors during lithium electrochemical intercalation into graphite in the entropy curve and the crystal structure, especially, during the stages from 2 to 1 transition at $x = 0.5$ in Li_xC_6. The entropy first decreases monotonously, then re-increased sharply at the transition. The average interlayer spacing displays a hysteresis during intercalation and de-intercalation and departs from linearity. The results are discussed in relation with a contribution of the vibrational entropy and possible occurrence of intermediary phase(s) between the two lithium-rich intercalation stages.

Keywords: Graphite; Lithium; Entropy; Stage; Phase transition

1. Introduction

The chemistry of lithium-ion batteries is based on the lithium-ion shuttling between the graphite negative electrode and the transition metal(s) oxide positive electrode. The overall reaction can be schematized as:

$$Li_xC_6 + Li_yMO_2 \leftrightarrow 6C + Li_{y+x}MO_2 \quad (1)$$

Due to differences in the chemical potential of lithium in the Li_xC_6 and $Li_{y+x}MO_2$ materials, the operating voltage of the battery is a high 4 V.

The lithiated graphite electrode has many attractive features that have made it the best choice for negative electrode in commercial batteries. These include high mass and volume capacity, low operating voltage, long cycle life and good safety. From the crystal chemistry point of view, lithiation of graphite undergoes a characteristic series of phase transitions called stages. In graphite-intercalation compounds (GICs), an intercalation stage describes the 2D stacking sequence of the lithium layers between the graphene layers. The stage number is the number of periodically stacked graphene layers between two adjacent intercalated layers. Starting from pure graphite, successive stages are formed as the lithium concentration increases. One way to intercalate lithium into graphite is by electrochemical cathodic polarization of a graphite electrode in a Li organic liquid or solid-state polymer electrolyte cell. Based on in situ and ex situ X-ray diffractometry, the stages that form as the lithium concentration increases are: dilute stage 1, stages 4 and 3, liquid-type stage 2 and stages 2 and 1 [1–4]. The composition-induced stage transitions occur at relatively well-defined 'x' values around 0.05, 0.13, 0.18, 0.25 and 0.5, respectively. In dilute stage 1, lithium is randomly distributed between the graphene layers, which causes a slight shift of the (0 0 2) main peak of hexagonal graphite to lower diffraction angles. Liquid-type stage 2 has lithium in every other layer, with no long-range in-plane ordering. This contrasts with the stage 2 compound of nominal composition $Li_{0.5}C_6$ (LiC_{12}) in which the lithium forms an ordered array with the characteristic hexal structure [5]. The same hexal structure occurs in stage 1 LiC_6 in which lithium occupies each van der Waals gap between the graphene sheets.

Fig. 1 shows typical lithiation/de-lithiation voltage profile curves obtained with graphite under a low galvanostatic cycling regime (i.e. C/100 rate) [6]. It shows plateaus

* Corresponding author. Tel.: +1 626 395 4496.
E-mail address: yazami@caltech.edu (R. Yazami).

0378-7753/$ – see front matter © 2005 Elsevier B.V. All rights reserved.
doi:10.1016/j.jpowsour.2005.05.087

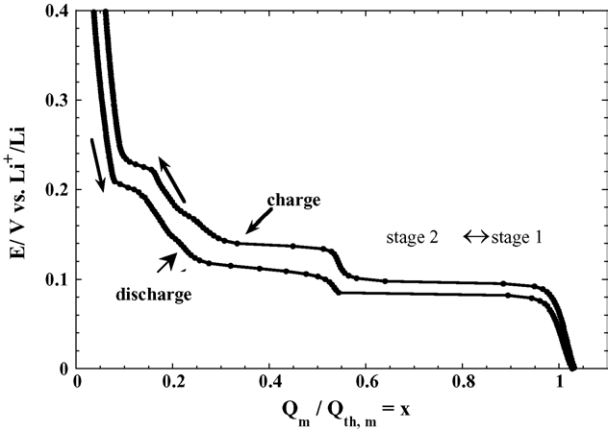

Fig. 1. Voltage vs. composition curves during the graphite electrode lithiation and de-lithiation at *C*/100 rate after Ref. [6].

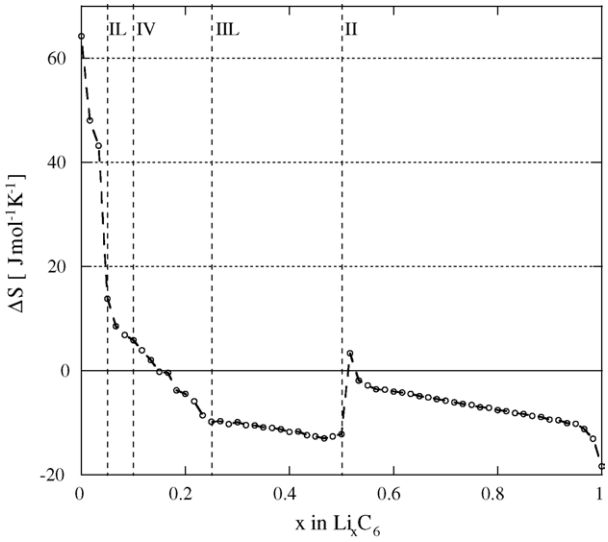

Fig. 2. The entropy of lithium-intercalation into natural graphite. The dashed lines delimit pure dilute stages 1, IV, II L and II.

and semi-plateaus corresponding to the stage transitions described above. A flat plateau is the signature of a two-phase system as in the case in the composition range of $0.5 < x < 1$. It has been well-accepted that the plateau is related to a two-phase system that is a mixture of stage 2 LiC_{12} and stage 1 LiC_6 phases following the equilibrium reaction:

$$LiC_{12} + yLi \leftrightarrow 2y\,LiC_6 + (1-y)\,LiC_{12} \quad (2)$$

According to Eq. (2), the fraction of each phase should vary linearly with lithium-intercalated beyond LiC_{12}.

In this paper, we present results from independent studies on the stages from 2 to 1 transition area that shows some unexpected features (anomalies). The results are obtained by entropy measurements ($\Delta S(x)$) and in situ X-ray diffractometry (XRD). The aim is to understand the mechanism of stage transition dealing with the observed anomalies.

2. Experiments and results

2.1. The entropy anomaly

Coin-type half cells with metallic lithium as the counter (and reference) electrode and natural graphite as the working electrode were used for the electrochemical study. The electrolyte consisted of a molar solution of $LiPF_6$ in equivolumic mixture of ethylene carbonate (EC) and dimethyl carbonate (DMC) [5]. The cell was cycled several times between 1.5 and 0 V.

We used the temperature dependence of the open-circuit voltage (OCV) at constant composition x in Li_xC_6 to measure the entropy variation $\Delta S(x)$ expressed by:

$$\Delta S(x) = F\frac{\partial(\mathrm{OCV}(x))}{\partial T}|_x \quad (3)$$

A program controlled an Agilent 3633 power supply, which provided current to a Peltier plate in order to make the temperature steps. The program also controlled the acquisition of the open circuit voltage along with the temperature. An Agilent 34,970, 6.5-digit multimeter accurate to 10 μV was used for that purpose. Two RTD elements accurate to 0.1 °C were attached to the plate and the cells to monitor their temperatures. A four-channel Arbin BT4+ discharged the test cells to a chosen composition, which were then allowed to equilibrate for 8 h before temperature cycle being automatically launched. The temperature range used during this cycle varied from room temperature to 12 °C, in 2 °C steps. In this range, self-discharge is very low and can be neglected during measurement time [7]. However, even after 8 h rest, some potential drift of the order of 100 μV during the 2 h temperature cycles still occured and was substracted by the program from the experimental data to be as close as possible to the thermodynamic equilibrium.

Fig. 2 shows the entropy curve obtained during the lithiation process. Starting from a high and positive value of 60 J (mol K)$^{-1}$ at $x \sim 0$, $\Delta S(x)$ decreases steadily, changes in sign and makes a first plateau between $x = 0.25$ and 0.5. It reaches a local minimum of about -15 J (mol K)$^{-1}$ at $0.45 < x < 0.5$. Then, $\Delta S(x)$ suddenly increases at $x \sim 0.5$ and takes a positive value; then, it makes a slowly decreasing plateau before dropping sharply in the $x = 0.95$–1 composition range.

2.2. The crystal structure anomaly

In situ X-ray diffraction was performed on a coin-type cell with a 4 mm × 6 mm Kapton window coated with conductive thin copper layer. The electrolyte consisted of a molar solution of $LiPF_6$ in equivolumic mixture of ethylene carbonate and dimethyl carbonate [5]. The graphite electrode was pressed against the Kapton window so as to be reached by

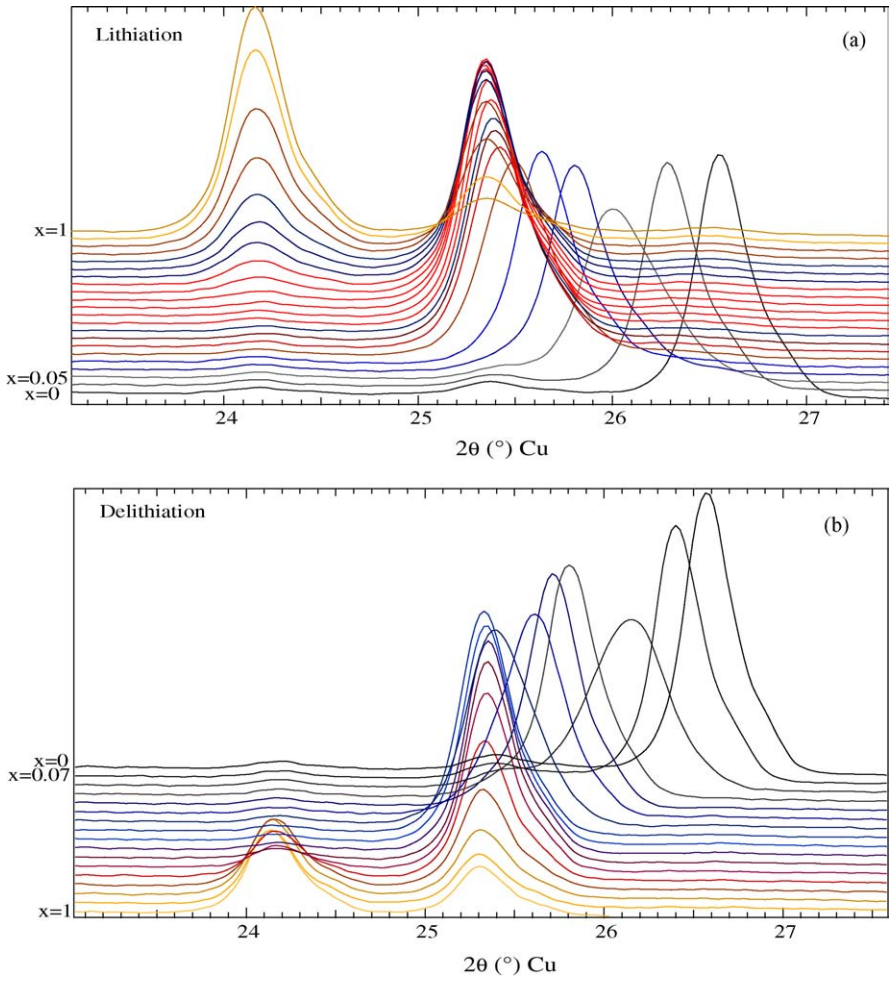

Fig. 3. XRD (*w*/Cu Kα) spectra during: (a) lithiation and (b) de-lithiation cycle of graphite under *C*/20 rate. The spectra were taken for 5 min after each hour charge or discharge.

the X-ray beam. After several lithiation/de-lithiation cycles under a *C*/10 rate between 1.5 and 0 V, the cell was fully de-lithiated up to 1.5 V. The cycle capacity achieved with the graphite electrode is about 360 mAh g^{-1}. The cell was then re-lithiated under a slower rate of *C*/20. XRD patterns were taken for about 5 min every hour while the cell is under continuous discharge. As a result, the lithium composition x in Li_xC_6 was incremented by 0.05 between two successive XRD scans.

Fig. 3 shows the evolution of the XRD spectra during the discharge (lithiation, Fig. 3a) and the charge (Fig. 3b). The diffraction angle area shown is around the strongest peaks (i.e. the 0 0 2 of graphite and stage 2 and the 0 0 1 of stage 1). Starting from fully de-lithiated graphite with 0 0 2 peak at around 26.6° (d_{002} = 3.35 Å, Cu Kα radiation), the peak shifted continuously to lower angles until it reached about 25.2° at x = 0.33. This angle is the one of the 0 0 2 stage 2 compound. During this shift, the peak broadens in two regions, indicating a partial phase separation of the dilute stages 1–4 transition and stage 4 to liquid-type stage 2. The peak broadening occurs around $2\theta = 26°$ and 25.5°, respectively. However, the discharge rate was certainly too fast in this experiment to clearly distinguish two peaks in these domains.

The angular position of the peak then remained almost unchanged. No other peak appeared in the $0.5 < x < 0.7$ composition domain, where stage 1 is expected to form according to the stages from 2 to 1 two-phase model. Such a model has been widely used in the literature to explain the flat voltage plateau in the $0.5 < x < 1$ composition range. It was only after $x > 0.7$ that a new peak at $2\theta \sim 24°$ could be noticeable. The latter is the 0 0 1 peak of stage 1 corresponding to d_{001} = 3.71 Å. As x increased from 0.7 to 1, the 0 0 2 peak of stage 2 decreased in intensity while the 0 0 1 peak of stage 1 increased.

During lithium de-intercalation, the peaks intensities varied in opposite direction. However, the decrease rate of the 0 0 1 peak is lower at the beginning of this process than its increase rate during intercalation. In order to illustrate this hysteretic behavior, we calculated the average interlayer spacing ⟨d(x)⟩ based on the integrated 0 0 s peak intensities of stage s. for pure graphite, we took the 0 0 2 peak intensity.

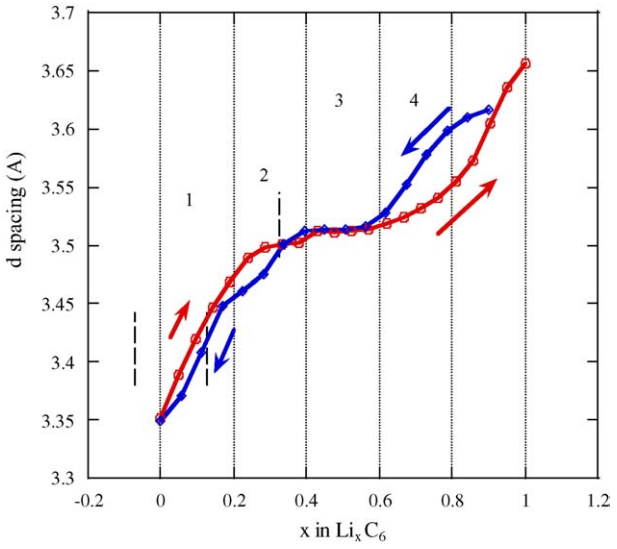

Fig. 4. Composition dependence of the average graphene interlayer spacing during the lithium-intercalation and de-intercalation.

Taking $\alpha(s)$ the fraction of stage s in the mixture, $\langle d(x)\rangle$ is given by:

$$\langle d(x)\rangle = \sum_s \alpha_s \frac{3.71 + 3.36(s-1)}{s} \quad (4)$$

$$\sum_s \alpha_s = 1 \quad (5)$$

Fig. 4 displays the composition dependence of $\langle d(x)\rangle$ during intercalation and de-intercalation. This curve seems to feature four distinguishable domains:

(1) $0 < x < 0.15$, where $\langle d(x)\rangle$ varies linearly with almost no hysteresis;
(2) $0.16 < x < 0.33$: a small hysteresis appears with $\langle d(x)\rangle$ is slightly higher during intercalation than de-intercalation;
(3) $0.33 < x < 0.5$: $\langle d(x)\rangle$ is almost constant around 3.51 Å;
(4) $0.5 < x < 1$: strong hysteresis, where $\langle d(x)\rangle$ is lower during intercalation than during de-intercalation.

3. Discussion

We attributed the sudden increase in entropy at $x \sim 0.5$, where stage 1 should begin to form two combined contributions from configurational and vibrational entropy [8]. Configurational entropy goes with in-plane or the out-of-plane lithium vacancy 'disorder'. This translates into either the formation of lower Li density layers or the presence of Li stacking faults. Indeed a possible mechanism of the stage 1 phase formation may involve a 'dilute lithium layer' (noted dil-Li) in similar way than in dilute stage 1 that forms at early stages of the graphite lithiation. Such a compound would have alternating 'normal' Li layer (Li) with the hexal structure and a dilute lithium layer following the sequence (Li)–G–(dil–Li)–G. Fig. 5 illustrates the structure of such pseudo stage 1 compound. Another source of disorder is the formation of "fractionary" stages, such as stages 3/2 and 4/3 [9]. The latter have the following stacking: (Li)–G–(Li)–G–G and (Li)–G–(Li)–G–G–(Li)–G, respectively. Fig. 5 illustrates the fractionary stages as possible path during the formation of stage 1, the other path involves the pseudo stage 1 formation. A combination of fractionary stages may also be considered to deal with the lithium layers stacking disorder during the early formation of stage 1. The most likely fractionary stages are the $\frac{n+1}{n}$; $n > 1$ stages, which consist of a periodic stacking of n lithium layers separated by $n+1$ carbon layers. In

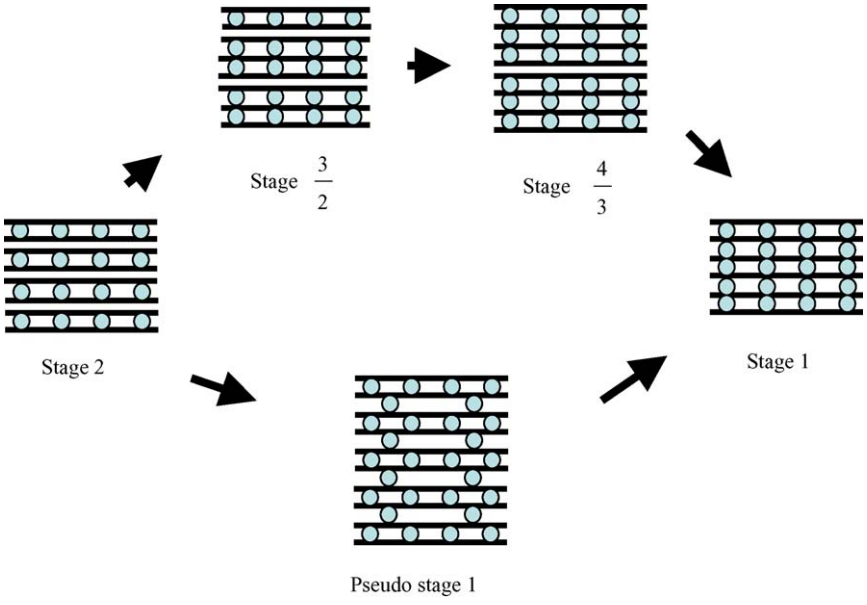

Fig. 5. Possible paths of intermediary phases between stages 2 and 1.

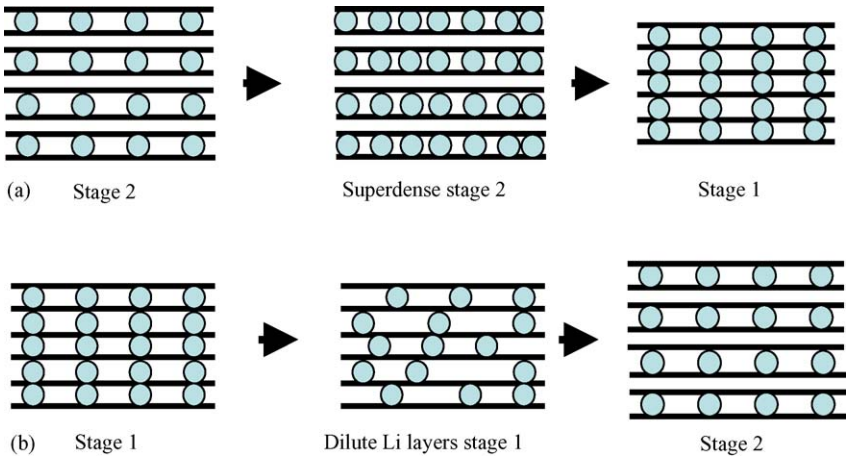

Fig. 6. Schematic representation of: (a) the stage 2 → stage 1 transition through superdense stage 2 compound, such as $Li_{1.5}C_{12}$ (or $Li_{0.75}C_6$) and (b) stage 1 → stage 2 transition involving dilute stage 1 compound.

such a phase, the periodicity along the *c*-axis is:

$$c = 3.35 + n3.71\,(\text{Å}) \tag{6}$$

The strongest X-ray diffraction line is then the $(0\,0\,n+1)$ line, with corresponding reticular distance $d_{(0\,0\,n+1)}$ of:

$$d_{(0\,0\,n+1)} = \frac{3.35 + 3.71n}{n+1} \tag{7}$$

and Bragg diffraction angle 2θ of:

$$2\theta = 2\,\text{Arc sin}\,\frac{(n+1)\lambda}{2(3.35 + 3.71n)} \tag{8}$$

The Bragg diffraction angle 2θ is a decreasing function of *n* and varies between $2\theta \sim 25.2^\circ$ and $\sim 24^\circ$ corresponding to the pure stage 2 ($n = 1$) and pure stage 1 ($n = \infty$), respectively. We did not observe any continuous shift of the 0 0 2 peak of stage 2 towards lower angles nor the appearance of the 0 0 1 peak of stage 1 in the $0.5 < x < \sim 0.7$ composition range. Although we reported on the existence of lithium composition gradient within the electrode, which makes the sample area observed by X-ray appear richer in the stage 2 phase [10], the composition range of $\Delta x \sim 0.2$, where stage 1 compound is not observed is rather large. This strongly suggests that additional lithium may at first intercalate in the lithium-filled layer rather than in the adjacent empty layer in stage 2. In this case, denser lithium layer with Li_2 pairs may form, which preserves the stage 2 structure. Superdense stage 2 domains may act as a nucleation phase in the kinetics process of stage 1 formation, a mechanism of which is illustrated in Fig. 6a.

The hysteresis in the average interlayer spacing in the $0.5 < x < 1$ composition range during intercalation and de-intercalation in Fig. 4 suggests that different crystallographic paths are followed during intercalation and de-intercalation. As in the latter, the interlayer spacing is higher than in the former, it is very likely that starting from LiC_6, lithium is de-intercalated from each equivalent layer, which preserves the stage 1 stacking sequence as sketched in Fig. 6b. This implies that at the early stage of de-intercalation, the lithium layers have cation vacancies, which may be a 'mirror phase' to dilute stage 1 formed at early steps of intercalation. Li vacancies would then form a dilute stage 1 compound keeping almost constant the average interlayer spacing.

In superdense LiC_n phases ($n < 6$) (see Fig. 7 for in-plane structure illustration), the average Li–Li distance in a Li_2 pair is of 2.46 Å, much lower value than 4.26 Å in the hexal structure of normal stages 2 and 1 compounds and still lower than that in bcc lithium of 3.04 Å. A strong Li–Li repulsion is taking place in stage 1 superdense phases which makes them unstable, a reason why they cannot be formed by electrochemical intercalation under normal pressure and temperature conditions [11–13]. Rather, they are typically obtained under high pressure/high temperature synthesis conditions [14] or by ball milling [15]. Stage 1 superdense LiC_2 decomposes to intermediary and "kinetically" more stable stage 1 phases, such as Li_7C_{24} or $Li_{11}C_{24}$ [16]. The ultimate phase of decomposition is LiC_6. All superdense phases described in the literature have the lithium sub-lattice commensurate with that of graphite, with short Li–Li distances. The latter are at origin of metastability as the electrostatic Li–Li repulsion becomes dominant. Should superdense stage 2 form as intermediary phase between stages 2 and 1, its stabilization may go through a change in the Li in-plane ordering. This may involve a non-commensurate Li sub-lattice having a Li–Li distance lying between 2.46 and 4.26 Å of LiC_2 and LiC_6, respectively. More work is necessary to confirm the formation of superdense stage 2 and eventually the type of lithium in-plane organization.

The vibrational entropy is related to a disorder originated from the Li vibrational motion about the equilibrium position at the center between two adjacent carbon hexagons. Such a motion can be decomposed in two terms: a vibration along the *c*-axis and a vibration within the medium plane between the graphene layers [8]. Each vibration mode can be defined by its Debye temperature, $\theta_\perp$ and $\theta_{//}$ for movement perpendicular and parallel to the graphene plane, respectively. The

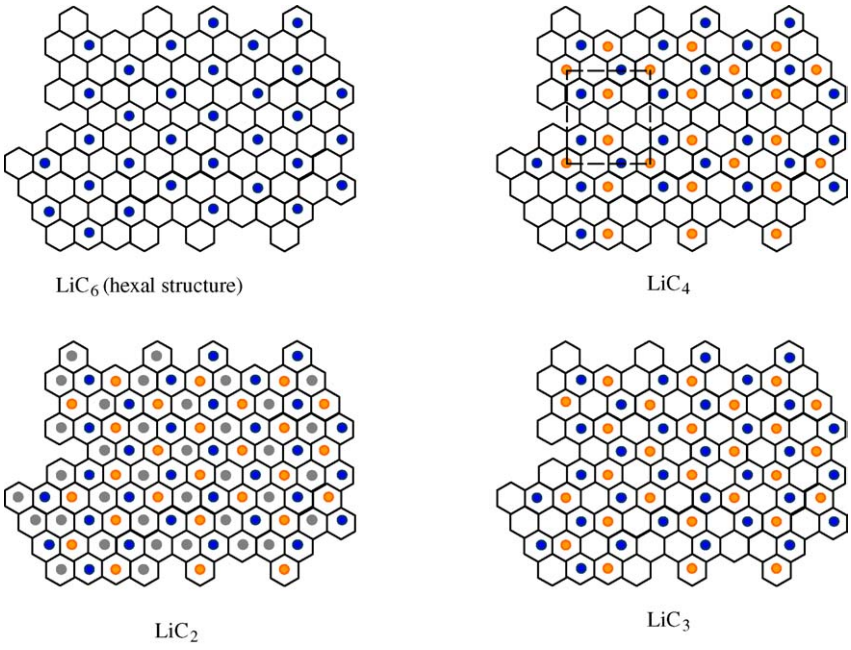

Fig. 7. In-plane organization of the LiC_n ($n \leq 6$) phases including some superdense phases.

difference of vibrational entropy of lithium in the stages from 2 to 1, compounds can be approximated in this Debye model by [17]:

$$\Delta S_{\text{vib}} = R\left(\ln\left(\frac{\theta_{//1}}{\theta_{//2}}\right) + 2\ln\left(\frac{\theta_{\perp 1}}{\theta_{\perp 2}}\right)\right) \quad (9)$$

where 1 and 2 indexes refer to the Debye temperature in stages 1 and 2, respectively. These data were determined by inelastic neutron-scattering measurements [18]. The total entropy variation using Eq. (9) is in the order of about 2 J $(\text{mol K})^{-1}$, which accounts for 10–15% of the total entropy and should not be neglected. Note that the Debye approach neglects a large part of the phonon spectrum, and therefore, may not account for the total vibrational entropy.

4. Conclusion

Independent entropy and XRD measurements show anomaly behaviors at the stage 2 ↔ stage 1 phase transition. We found converging evidences that for compositions between $0.5 < x < 1$ in Li_xC_6, the compound is not consisting with a proportional mixture of stages 2 and 1 as Eq. (2) may suggest. The Li composition gradient within the electrode thickness may in part explain the hysteresis in the stages 2 to 1 transition. Our results are also consistent with the formation of intermediary phases, such as superdense stage 2 and Li vacancy containing stage 1. These phases may act as the nucleation steps in the phase transition. The occurrence of fractionary stages could also account for increased configurational entropy at transition. We also showed that the crystallographic paths may be different during the transition one way the other which may involve intermediary states with very close total energy.

We are currently undertaking first-principle calculations on the Li_xC_6 system in order to explore the energy favored paths during the stages 2 to 1 transition and determine the corresponding thermodynamic state functions [19].

Acknowledgements

The authors thank Prof. Brent Fultz from Caltech for fruitful discussions. They acknowledge the financial supports from CNRS, France and the US-DOE through Basic Energy Sciences Grant DE-FG03-00ER15035.

References

[1] R. Yazami, P. Touzain, J. Power Sources 9 (1983) 365.
[2] J.R. Dahn, Phys. Rev. B 44 (1991) 9170.
[3] D. Billaud, F.-X. Henry, P. Willman, J. Power Sources 54 (1995) 207.
[4] D. Aurbach, B. Markovsky, I. Weissman, E. Levi, Y. Ein-Eli, Electrochim. Acta 45 (1999) 67.
[5] D. Guérard, A. Hérold, Carbon 13 (1975) 337.
[6] A. Martinent, Ph.D. Thesis, University of Grenoble, 2001.
[7] Y. Reynier, R. Yazami, B. Fultz, IEEE 02TH8576 Long Beach (2002) 145.
[8] Y. Reynier, R. Yazami, B. Fultz, J. Power Sources 119 (2003) 850.
[9] C.D. Fuerst, J.E. Fischer, J.D. Axe, J.B. Hastings, D.B. McWhan, Phys. Rev. Lett. 50 (1983) 357.
[10] Y. Reynier, R. Yazami, B. Fultz, J. Power Sources, in press.

[11] R. Yazami, A. Cherigui, V.A. Nalimova, D. Guérard, Proceedings of the 182nd Meeting of the Electrochemical Society, Toronto, Canada, 1992, p. 17.
[12] C. Bindra, V.A. Nalimova, D.E. Sklowsky, Z. Benes, J. Fischer, J. Electrochem. Soc. 145 (1998) 2377.
[13] R. Tossini, R. Janot, F. Nobili, D. Guèrard, R. Marassi, Electrochem. Acta 48 (2003) 1419.
[14] K.N. Semenenko, V.V. Adveev, V.Z. Mordkovich, Doklady An. SSSR 271 (1983) 1402;
V.A. Nalimova, V.V. Adveev, K.N. Semenenko, High Pressure Res. 6 (1990) 11.
[15] D. Guérard, R. Janot, J. Phys. Chem. Sol. 65 (2004) 147.
[16] J. Conard, V.A. Nalimova, D. Guérard, Mol. Cryst. Liq. Cryst. 245 (1994) 25.
[17] P.D. Bogdanoff, B. Fultz, Philos. Magn. B 79 (1999) 753.
[18] R. Moreh, N. Shnieg, H. Zabel, Phys. Rev. B 44 (1991) 13111.
[19] J.-S. Filhol, F. Lemoigno, R. Yazami, M.-L. Doublet, Phys. Rev. Lett., under review.